ACS Catalysis

Research Article

pubs.acs.org/acscatalysis

Carbon Corrosion in Proton-Exchange Membrane Fuel Cells: From Model Experiments to Real-Life Operation in Membrane Electrode Assemblies

Luis Castanheira,[†,‡] Laetitia Dubau,[†,‡] Michel Mermoux,[†,‡] Gregory Berthomé,[§,∥] Nicolas Caqué,[⊥] Elisabeth Rossinot,[⊥] Marian Chatenet,[†,‡,¶] and Frédéric Maillard*[,†,‡]

[†]University of Grenoble Alpes, LEPMI, F-38000 Grenoble, France

[‡]CNRS, LEPMI, F-38000 Grenoble, France

[§]University of Grenoble Alpes, SIMAP, F-38000 Grenoble, France

[∥]CNRS, SIMAP, F-38000 Grenoble, France

[⊥]Axane, 2 rue de Clémencière, BP 15, 38360 Sassenage, France

[¶]Member of the French University Institute, IUF, Paris, France

Supporting Information

ABSTRACT: The electrochemical oxidation of carbon is a pivotal problem for low-temperature electrochemical generators, among which are proton-exchange membrane fuel cells (PEMFCs), and (non)aqueous-electrolyte Li−air batteries. In this contribution, the structure-sensitivity of the electrochemical corrosion of high-surface area carbon (HSAC) used to support catalytic materials in PEMFC electrodes is investigated in model (liquid electrolyte, 96 h potentiostatic holds at different electrode potentials ranging from 0.40 to 1.40 V at T = 330 K) and real PEMFC operating conditions (solid polymer electrolyte, 12,860 h of operation at constant current). Characterizations from Raman spectroscopy demonstrate that the disordered domains of HSAC supports (amorphous carbon and defective graphite crystallites) are preferentially oxidized at voltages related to the PEMFC cathode (0.40 < E < 1.00 V). Excursions to high electrode potential E > 1.00 V, witnessed during start-up and shut-down of PEMFC systems, accelerate this phenomenon and propagate the electrochemical oxidation to the graphitic domains of the HSAC. Thanks to X-ray photoelectron spectroscopy, a better understanding of the relationships existing between structural changes and carbon surface oxides coverage is also emerging for the first time.

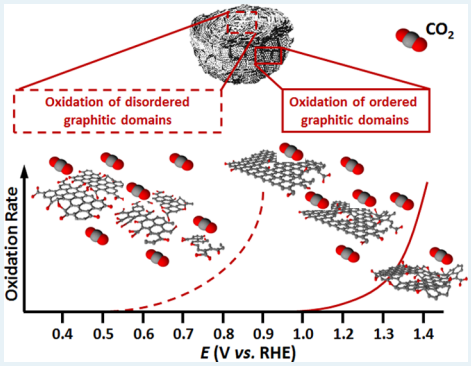

KEYWORDS: *proton-exchange membrane fuel cells (PEMFCs), durability of PEMFC materials, degradation mechanisms, carbon corrosion, catalyst support corrosion*

The increasing CO_2 concentration in the atmosphere and its consequences on our environment daily demonstrate the necessity to ensure sustainable development and clean energy production. In this regard, electrochemical generators are of prime interest since they allow decreasing the release of air pollutants. In particular, the proton-exchange membrane fuel cell (PEMFC), that uses hydrogen fuel (ideally of renewable origin) and oxygen from the air, can produce electricity in a clean and efficient manner. However, this technology still suffers from a decline of long-term electrical performance, mainly related to the degradation of the electrocatalytic materials (Pt-based nanoparticles supported on high surface area carbon, HSAC). The major degradation mechanisms of Pt/HSAC or Pt-M/HSAC (M being an early or late transition metal) electrocatalysts are well-established[1] and involve (i) the migration/agglomeration of the metal nanoparticles, (ii) the dissolution/electrochemical redeposition of metallic ions (Pt^{z+} and M^{y+}) in the catalytic layer (electrochemical Ostwald ripening), or (iii) in the proton-exchange membrane via chemical reduction by hydrogen crossing over from the anode to the cathode, and (iv) the electrochemical oxidation of the high surface area carbon support (carbon oxidation reaction - COR).

Early studies dealing with COR have been made in the context of phosphoric acid fuel cells (phosphoric acid electrolyte, 423 < T < 493 K).[2−5] Because PEMFC systems operate at much lower temperature (T = 343−353 K), the COR was believed to be insignificant in PEMFC operating conditions, which was proven incorrect.[6,7] Indeed, the low carbon dioxide/carbon standard potential $E^0_{CO_2/C}$ = 0.207 V vs the normal hydrogen electrode (NHE) renders it thermody-

Received: April 4, 2014
Revised: May 22, 2014
Published: June 13, 2014

namically possible in a PEMFC. The COR is mostly a concern at the cathode,[8,9] in particular during start/stop or fuel starvation events, where the electrode potential may reach up to 1.5 V vs the reversible hydrogen electrode (RHE).[10−12] The localized fuel starvation events, such as those caused by blocking of a fuel channel or differences in H_2 partial pressure under the channel or the land during PEMFC start-up, also cause localized but severe carbon corrosion in PEMFC cathode electrodes.[13]

The mechanism of the COR is still not fully established but is believed to occur via the formation of carbon surface oxides and the evolution of CO_2.[3,6,14,15] The carbon surface oxide groups include but are not limited to phenols, ethers, ketones, and carboxylic acids, and are referred to as CO_{surf} in what follows.[2,16] Due to the observed power-law dependence of the COR rate and the increasing faradaic efficiency of CO_2 evolution over time,[3] Kinoshita et al. suggested that these groups act as passivation species for the reaction. The COR kinetics is strongly affected by the potential, the temperature, the morphology, the structure, and the surface properties of carbon materials.[15,17−19] It is catalyzed by the presence of Pt nanoparticles,[7,8,20,21] most likely through the spillover of CO_{surf} species to the surface of the Pt nanoparticles and their further oxidation into CO_2 at potentials between 0.60 and 0.80 V vs RHE, where oxygenated species are nucleated on the catalytic surface.[9] The consequences of the COR involve (i) the agglomeration and/or detachment of the metal nanoparticles, which result in lower catalyst utilization and decrease the electrochemically active surface area (ECSA),[22−24] (ii) the decrease of the electrode porosity,[23] and (iii) the emergence of water management difficulties due to the growth of hydrophilic CO_{surf} groups.[6] The two latter processes yield increased mass-transport issues in the electrodes and are therefore particularly detrimental to their long-term performances.[25]

The COR is currently studied by applying potentiostatic polarization for several hours at electrode potentials ≥1.4 V vs RHE,[19,26,27] so as to mimic the excursion to high potential that a PEMFC cathode experiences during start/stop or fuel starvation events. These accelerated stress tests (ASTs) provide an efficient way to screen different carbon supports, but they level-off their resistance to corrosion and provide poor mechanistic perspective. In addition, these excursions to high potential are far from the conditions that a PEMFC experiences during the major part of its life; for example, during automotive fuel cell operation, the cathode potential lies between 0.70 V vs RHE and the open-circuit potential (0.95 V vs RHE),[28] i.e. a much narrower potential range than the one investigated in ASTs. This statement is particularly true during stationary operating conditions for which the cathode mostly experiences electrode potentials lower than 0.90 V vs RHE.[29−32] To the best of our knowledge, the degradation mechanisms of HSAC supports in these operating conditions have never been investigated and are the focus of the present study.

Herein, a state-of-the-art Pt/HSAC electrocatalyst was subjected to long-term (96 h) polarization at different electrode potentials ranging from 0.40 to 1.40 V vs RHE and T = 330 K. The structural changes of the Pt/HSAC electrocatalyst were followed by Raman spectroscopy, while X-ray photoelectron spectroscopy (XPS) provided a chemical analysis of their surface. Finally, the observations made in model conditions were compared to those obtained during a long-term stationary PEMFC test (i = 0.25 A.cm^{-2}, 0.65 V < E_{cell} < 0.77 V, T = 335 K, t = 12,860 h, 250 start/stop events).

EXPERIMENTAL SECTION

Electrocatalysts. The electrocatalyst used in this study was a Pt catalyst supported on high-surface-area carbon (HSAC) with a weight fraction (wt %) of 40% (TEC10E40E), which was supplied by Tanaka Kikinzoku (TKK). The carbon support features a high surface area (800 m^2 g^{-1}), and the surface-averaged Pt particle size is 2.3 nm. The electrocatalyst was used as-received without any further treatment.

Electrochemical Measurements. The solutions were daily prepared from ultrapure water (MQ grade, 18.2 MΩ cm, 1−3 ppb TOC) and H_2SO_4 (Suprapur, Merck). The electrolyte was a 0.1 M H_2SO_4 aqueous solution purged with argon (Ar > 99.99%, Messer). All the glassware was first cleaned by immersion in a H_2SO_4:H_2O_2 mixture overnight and thoroughly rinsed with MQ-grade water. The electrochemical characterization of the 40 wt % Pt/HSAC electrocatalyst and the potentiostatic tests were conducted in two separate four-electrode electrochemical cells, a characterization and a degradation cell, both thermostated at T = 330 K. A homemade rotating disk electrode (RDE) tip was used as a working electrode. The counter-electrode was a Pt foil, and the reference electrode, a mercury sulfate electrode—MSE, Hg|Hg_2SO_4|K_2SO_4 (saturated, aqueous)—connected to the cell via a Luggin capillary. This reference electrode was calibrated periodically by measuring its potential difference with a reversible hydrogen electrode (RHE), which was systematically 0.72 V vs RHE. All the potentials reported in this study were referenced on the RHE scale. A Pt wire connected to the reference electrode was used to filter the high-frequency electrical noise and to avoid disturbing the low-frequency electrical measurements.

Preparation of the Catalytic Layers. A suspension with a concentration of 0.735 $g_{Pt/C}$ L^{-1} of Pt/C, composed of 5 wt % Nafion solution (Aldrich), MQ-grade water, and 40 wt % Pt/HSAC, was ultrasonically treated for 15 min to obtain a well-dispersed ink. Before each degradation test, the ink was sonicated for 6 min. Two calibrated drops of 20 μL additions of this ink were deposited onto a homemade RDE made of glassy carbon (Sigradur, 0.196 cm^2) and Teflon resulting in a Pt loading of 60 μg_{Pt} cm^{-2}. After each drop was deposited, the ink was dried for 5 min in air at T = 383 K to ensure evaporation of the water and the solvents of the Nafion solution, resulting in a so-called "porous" RDE. The working electrode was immersed/withdrawn into/from the electrochemical cell at controlled electrode potential E = 0.40 V vs RHE.

Electrochemical Characterization. Ten cyclic voltammograms at v = 20 mV s^{-1} and one cyclic voltammogram at v = 100 mV s^{-1} were first recorded between E = 0.05 and 1.23 V vs RHE to obtain the characteristic voltammetric response of 40 wt % Pt/HSAC. The ECSA of the fresh Pt/HSAC electrocatalyst was measured from CO-stripping voltammograms performed at v = 100 mV s^{-1}. The CO saturation coverage was established by bubbling CO for 6 min and purging the solution with Ar for 45 min, while keeping the electrode potential at E = 0.10 V vs RHE. It was assumed that the electrooxidation of an adsorbed CO monolayer requires 420 μC per cm^2 of Pt. After the characterization, the electrode was then withdrawn from the solution at controlled electrode potential E = 0.40 V vs RHE and then transferred to the degradation cell with the electrode surface protected by a drop of electrolyte.

Accelerated Stress Test Protocol. The accelerated stress tests performed in this study consisted of potentiostatic

dx.doi.org/10.1021/cs500449q | ACS Catal. 2014, 4, 2258−2267

measurements performed at E = 0.40, 0.50, 0.60, 0.70, 0.80, 0.90, 1.00, 1.20, 1.30, or 1.40 V vs RHE for 96 h. The changes in the electrochemically active surface area (ECSA, cm^2_{Pt}) during the ASTs were monitored via CO_{ad} stripping coulometry (after 6, 24, 48, 72, and 96 h) in the characterization cell. Before the CO_{ad} stripping, five cyclic voltammograms at 100 mV s^{-1} and a cyclic voltammogram at 20 mV s^{-1} were recorded to characterize the surface reactivity of Pt/HSAC.

PEMFC TESTING

A 110-cell PEMFC stack using Pt/C at the anode and at the cathode was operated at constant current density (j = 0.25 A cm^{-2}) for t = 12,860 h at 333 < T < 338 K. The electrocatalytic materials, the chemical nature of the ionomer contained in the catalytic layers, and the proton-exchange membrane are proprietary and cannot be described. The catalytic layers were catalyst-coated membranes (geometric area 86 cm^2). The cathode was fed with humidified air (60−75% relative humidity (RH), close to the atmospheric pressure, gas stoichiometry of 2.5), and the anode was fueled with dry pure dihydrogen (0% RH, 1.35 bar abs., dead-end mode, corresponding to an average H_2 stoichiometry of ∼1.1). Air and H_2 purges were performed intermittently to remove the water produced at the cathode and the water and nitrogen that accumulate at the anode, respectively. Practically speaking, the air RH was fixed at the gas inlet by an adequate choice of the humidifier and cell temperature, and the air stoichiometry was doubled intermittently to allow air purges. The frequency and the duration of the air purge are proprietary and cannot be mentioned. The stack was disassembled at the end of life, and used for physical, chemical and electrochemical characterization. All the data presented in this study were obtained for electrocatalysts sampled in the cathode inlet region of the membrane electrode assembly (MEA), which is the region of harshest degradation in the present operating conditions.[33]

Raman Spectroscopy. Raman spectroscopy was used to examine the structure of the fresh and aged carbon supports. The Raman spectra were recorded *ex situ* using either a Renishaw RM1000 or a Renishaw In-Via spectrometer. The Raman spectra were obtained by excitation with the radiation from an argon LASER (514 nm) operated at approximately 5 mW. The detector was a Peltier-cooled charge coupled device camera, and the spectral resolution was 1 cm^{-1}. The measurements were performed with a ×50 ULWD objective and a 100 μm confocal aperture for both the sample illumination and collection of the scattered photons. For the sake of comparison, the Raman spectra of the Pt/HSAC electrocatalysts were normalized to the intensity of the peak at ∼1585 cm^{-1}, which corresponds to the band of the graphitic lattice. Curve fitting was performed with the software LabSpec. An accurate fitting of the Raman spectra considers the presence of five bands (Table 1).[34]

The changes in structure of the carbon support were followed by the variation of the mean crystallite size of the carbon particles, obtained with the Knight and White formula:[35]

$$L_a(\text{nm}) = 4.4 \times (I_{D1}/I_G)^{-1} \quad (1)$$

X-ray Photoelectron Spectroscopy (XPS). For XPS experiments, electrodes were prepared as for electrochemical experiments, i.e. the Pt/HSAC electrocatalyst was deposited onto a homemade RDE consisting of a glassy carbon tip (Sigradur, 0.196 cm^2) and Teflon. This tip was then removed from the RDE, fixed onto a molyblock and introduced into the XPS chamber within 1 h of the end of the AST. This procedure did not change the surface oxide coverage and chemical composition, as shown by Figure S1 in the Supporting Information (SI). The XPS patterns were obtained on a XR3E2 spectrometer (Vacuum Generator) equipped with a Mg Kα (1253.6 eV) X-ray source powered at 300 W (15 kV, 20 mA). The kinetic energies of the photoelectrons were measured using a hemispherical electron analyzer working in the constant pass energy mode (30.0 eV). The background pressure in the analysis chamber was kept below 10^{-9} to 10^{-10} mbar during data acquisition. The XPS data signals were taken in increments of 0.1 eV with dwelling times of 50 ms. Analyses were carried out at an angle 90° between the sample surface and the analyzer. High-resolution spectra envelopes were obtained by curve fitting of the XPS multiplex peaks using the software "Avantage" from ThermoScientific. Symmetric Gaussian−Lorentzian (90:10) product functions were used to approximate the line shapes of the fitting components with Shirley background corrections. The full width at half-maximum of the XPS envelopes was arbitrarily fixed at 1.7 ± 0.1 eV. To correct for any charging effect, all the binding energies were referenced to the graphene component (C−C) of the carbon C1s peak at 284.3 eV. The evolution of the oxygen content during the AST was monitored by dividing the peak areas of the O1s and the C1s signal (without the contribution of Nafion-related envelopes), after proper background subtraction, by their respective atomic sensitivity factors:

$$\text{ratio(O1s/C1s)} = \frac{I_{O1s}}{0.63} \times \frac{0.205}{I_{C1s}} \quad (2)$$

Table 1. Vibration Modes Observed on High Surface Area Carbon Supports with Raman Spectroscopy

band	Raman shift	vibration mode
G	∼1585 cm^{-1}	ideal graphitic lattice
D1	∼1350 cm^{-1}	disordered graphitic lattice−graphene layer edge
D2	∼1610 cm^{-1}	disordered graphitic lattice−surface graphene layer
D3	∼1495 cm^{-1}	amorphous carbon
D4	∼1190 cm^{-1}	polyenes, ionic impurities

RESULTS AND DISCUSSION

Figure 1 displays intermediate cyclic voltammograms (CVs) recorded during the ASTs. The electrochemical features obtained in the CVs depend on the polarization potential. When the potentiostatic AST was performed at E_{AST} = 0.40 V vs RHE, a broad oxidation peak (I > 0) can be distinguished in the potential range 0.5 < E < 0.8 V vs RHE. This redox peak is ascribed to the one-electron transfer on quinone/hydroquinone (Q/HQ) groups:[2]

$$C{=}O_{(s)} + H^+ + e^- \leftrightarrow C - OH_{(s)} \quad (3)$$

The larger electrical charge under this peak (positive-going potential sweep) relative to that measured on the pristine material points toward higher concentration of hydroquinone groups on the aged Pt/HSAC electrocatalyst surface. Similarly, "extra current" in the Pt surface oxide formation region (positive-going potential sweep, E > 0.80 V vs RHE) relative to what is observed on the fresh Pt/HSAC indicates that other

dx.doi.org/10.1021/cs500449q | ACS Catal. 2014, 4, 2258−2267

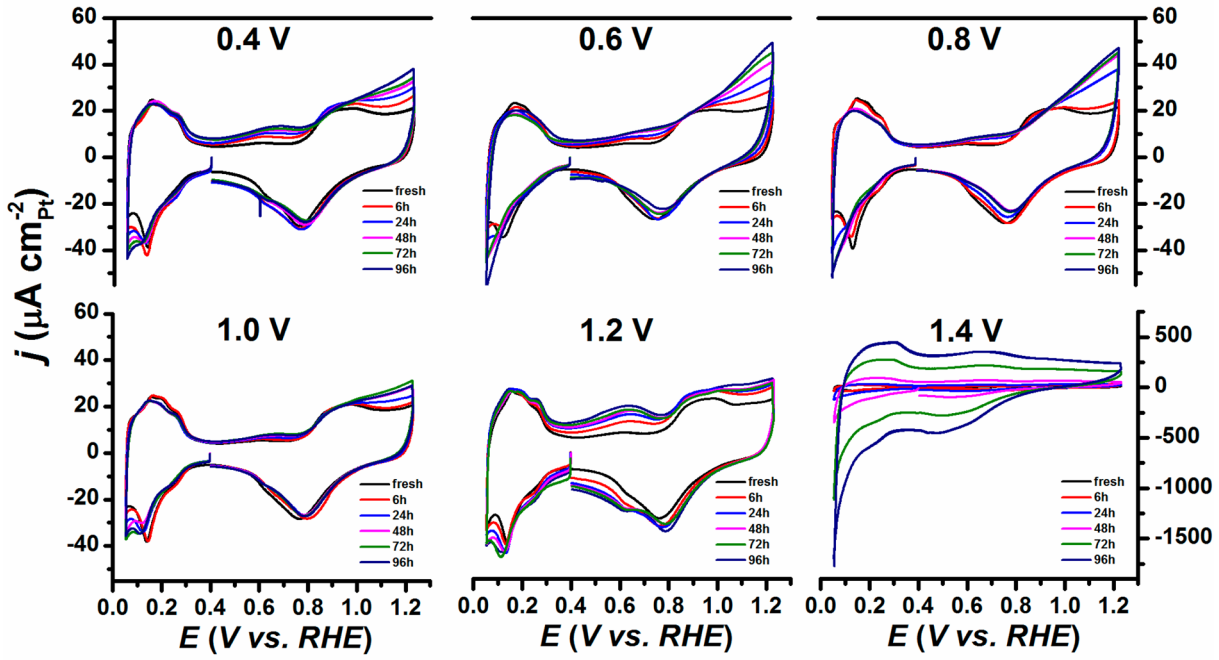

Figure 1. Intermediate characterization cyclic voltammograms measured on the Pt/HSAC electrocatalysts during the ASTs. The current is normalized to the real surface area estimated by CO_{ad} stripping coulometry. Electrolyte: 0.1 M H_2SO_4; ν = 0.020 V s^{-1}; T = 330 K.

COR intermediates were formed during the 96 h-polarization at E_{AST} = 0.40 V vs RHE (the under-potentially deposited hydrogen region of Pt (0.05 < E < 0.40 V vs RHE) being unchanged, this extra current does not originate from any Pt surface roughening).

Increasing the polarization potential to more positive values (0.40 < E_{AST} < 0.80 V vs RHE) results in a decrease of the currents related to electron transfer on Q/HQ groups, and suggests that these functional groups were oxidized during the 96 h-polarization. Concomitantly, the "extra-current" in the potential region of E > 0.80 V vs RHE is magnified, suggesting a larger surface concentration of CO_{surf} groups (that are not of the Q/HQ family). It is also interesting to note that the charge density associated with the under-potential deposition/desorption of protons on Pt depreciates with increasing values of E_{AST}. This may be rationalized by considering that CO_{surf} groups spill over from the HSAC support to the Pt nanoparticles, where they dehydrogenate, and form CO molecules that adsorb on Pt.[9] When the AST was performed in the potential interval of 0.80 < E_{AST} < 1.00 V vs RHE, the formation of surface oxides on Pt (via water splitting) facilitated the removal of the adsorbed CO molecules. Consequently, no change of the charge density in the H_{upd} adsorption/desorption region was observed in the intermediate characterization CVs. For E_{AST} > 1.00 V, remarkable features: (i) the increase of the current in the potential region 0.50 < E < 0.80 V vs RHE (reappearance of current ascribed to Q/HQ groups), (ii) the disappearance of the "extra-current" at E > 0.80 V vs RHE and (iii) the increase of the interfacial double-layer capacitance. Since the capacitance of a Pt/HSAC-based electrode is essentially fixed by the HSAC support, the larger double-layer capacitance points toward a more hydrophilic surface, and possibly an increase of the carbon support roughness (creation of structural defects).[30,36] Summing up, the electrochemical characterizations suggest that the nature and the concentration of oxygen-containing surface groups formed as COR intermediates strongly depend on the applied potential during the stationary AST. Structural and chemical changes were noticed in the intermediate characterization CVs at potentials as low as E_{AST} = 0.40 V vs RHE. These changes were magnified at E_{AST} ≥ 1.00 V vs RHE in the present experimental conditions (0.1 M H_2SO_4, T = 330 K).

Figure 2 displays the electrical charge of the quinone/hydroquinone (Q/HQ) peak for the fresh and the aged Pt/HSAC electrocatalysts. This charge was calculated from the positive-going potential sweep of the CV performed just before the CO_{ads} stripping characterization, and it was corrected from the double-layer contribution measured at E = 0.40 V vs RHE. For the sake of comparison, the electrical charge of the Q/HQ peak was also calculated using the methodology developed by Park et al. (Figure 2b).[37,38] Whatever the calculation procedure, an increased Q/HQ electrical charge was observed after 96 h of polarization at E_{AST} = 0.40 V vs RHE, followed by a progressive decrease for 0.40 < E_{AST} < 1.00 V vs RHE. Interestingly, the same trend is found above 1.00 V: a sharp increase was observed for E_{AST} = 1.2 V vs RHE, and a further increase in potential resulted into a decreased Q/HQ electrical charge. Figure 2c illustrates the dependence of the position of the Q/HQ peak on the AST polarization potential. Here again, the relationship is not monotonous: the peak potential first increased for 0.40 < E_{AST} < 0.80 V vs RHE, and then decreased until E_{AST} = 1.2 V vs RHE. Since CV is a dynamic technique, this trend is, to some extent, related to the dependence of the surface concentration of Q/HQ groups on the polarization potential. Previous studies also suggested that the peak potential of the Q/HQ redox couple varies with the number of aromatic rings neighboring these functional groups.[2]

These results hold significant importance for the understanding of HSAC degradation mechanisms. Indeed, they challenge the current view in the field that electrochemical oxidation of HSAC supports necessarily results in increasing concentration of Q/HQ groups. As shown in this study, the

dx.doi.org/10.1021/cs500449q | ACS Catal. 2014, 4, 2258−2267

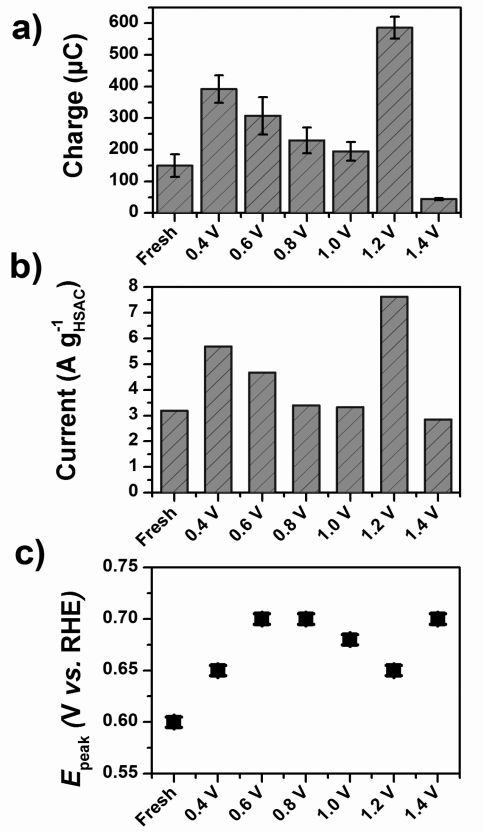

Figure 2. Characteristic features of the quinone−hydroquinone (Q/HQ) redox couple after 96 h of polarization at different electrode potentials: (a) coulometry (integration of the current between E = 0.40 and 0.75 V vs RHE) corrected from the interfacial double-layer contribution measured at E = 0.40 V vs RHE, (b) mass-normalized oxidation current, and (c) peak potential. Electrolyte: 0.1 M H_2SO_4; v = 0.020 V s^{-1}; T = 330 K.

surface concentration with Q/HQ groups at a given time depends (among others) on the polarization potential and the duration of the polarization. In some circumstances, such as a 96 h polarization at E_{AST} = 1.4 V vs RHE and T = 330 K, the surface concentration with quinone/hydroquinone groups was found to be smaller after the AST relative to that of the fresh sample.

The HSAC supports used in PEMFCs are composed of primary carbon particles (ranging from 10 to 100 nm) that are fused together via covalent bonds to form aggregates (100−800 nm), that finally pack into loosely bound agglomerates (1−100 μm).[16] Ordered (graphite-like), and disordered (defective graphite crystallites and amorphous carbon) domains are present within the primary carbon particles.[2,39,40] Figure 3 displays normalized Raman spectra of the fresh/aged samples, and the corresponding carbon mean crystallite size (L_a) estimated using the Knight and White formula.[35,41] The vibrational band appearing at ∼1350 cm^{-1}, namely the D1-band, is assigned to amorphous carbon domains and edges of the graphite crystallites, and the G-band at ∼1585 cm^{-1} is ascribed to the ordered graphite crystallites.[35] By means of deconvolution, the D2-band (at ∼1610 cm^{-1}) that is assigned to the defects present in the surface of the graphite crystallites, the D3-band (at ∼1495 cm^{-1}) and the D4-band (at ∼1190 cm^{-1}), which are ascribed to maxima in the vibrational density of states[42,43] or to polyenes and ionic impurities present in carbon blacks,[34] can be observed (Table 1). These bands are of great interest to understand the structural changes of model carbon supports having well-defined structure.[41,44−47] However, the high incertitude associated with the deconvolution of the Raman spectra into five bands makes them poorly useful for disordered HSAC supports such as that used in this study. Consequently, in what follows, only the variations in shape and in intensity of the D1-band and the G-band will be discussed. Therefore, any changes in the proportion of order/disordered domains in the sample will graphically result into modified D1-band intensity.

After 96 h of potentiostatic hold at 0.40 < E_{AST} < 1.00 V vs RHE, the Raman spectra feature a slow but continuous decrease of the D1-band intensity (Figure 3a), which suggests preferential oxidation of the more disordered domains of the HSAC support. At E_{AST} = 1.00 V vs RHE, the development of the D2-band intensity at ∼1600 cm^{-1}[45,46] suggests the formation of surface defects within the graphite crystallites. In addition, a new Raman band appears at ∼1760 cm^{-1} (inset of Figure 3a). This band is active in both infrared[48] and Raman spectroscopy,[49−51] and is ascribed to the C═O stretch vibration of carbonyl groups of carboxylic acids, or lactone groups. Its intensity increases with an increase in the polarization potential above 1.00 V vs RHE, suggesting that the HSAC surface becomes more oxidized. Along with the development of the C═O band, an increase in the polarization potential also causes a blue-shift of the D1- and D2-bands maxima relative to that of the fresh sample (5 cm^{-1} at maximum). This blue-shift translates changes in the effective force constant of the atomic vibrations, and may be rationalized by considering the adsorption of oxygen atoms on structural defects (oxygen atoms being more electronegative than carbon atoms, electron density will be transferred from the carbon atoms to the chemisorbed oxygen atoms). Similar results were reported for fluorinated graphene samples.[52]

In an early study, Tuinstra and Koenig[44] showed that the ratio of the D1 and G Raman band intensities (I_{D1}/I_G) is inversely proportional to the mean crystallite size L_a. Their results were confirmed later and generalized for different excitation wavelengths.[53,54] Using the Knight and White formula,[35] and the I_{D1}/I_G ratio determined from the best fits of the Raman spectra, the changes in the average carbon crystallite size (L_a) were estimated after each potentiostatic hold. The increase in L_a (see Figure 3b) indicates that amorphous carbon domains are preferentially oxidized in PEMFC operational potential range. Note, however, that different constants of proportionality between L_a and I_{D1}/I_G exist in the literature;[35,53,54] therefore, the L_a values should be considered with caution.

Figure 4 displays the O1s/C1s atomic ratio measured by XPS before/after the different ASTs, and the carbon surface oxide composition obtained by deconvolution of the C1s peak into different functional groups: C−C (sp^2 and sp^3-hybridized carbon atoms at 284.3 eV), C−O (hydroxyl, epoxy and ethers at 286.0 eV), C═O (carbonyl and/or quinone-like at 287.7 eV), O−C═O (carboxylic acid, lactone, anhydride at 289.4 eV) and C−F_2 and C-OF_2 and/or C−F_3 (Nafion ionomer at 291.3 and 293 eV respectively). The raw O1s and C1s spectra for each sample are provided in Supporting Information (see Figure S2 and Figure S3 in the SI). The O1s/C1s atomic ratio on the fresh sample is 0.33 ("C" conditions in Table 2). This ratio increased during the AST, but the trend is, again, nonmonotonous: the coverage with CO_{surf} species steadily

dx.doi.org/10.1021/cs500449q | ACS Catal. 2014, 4, 2258−2267

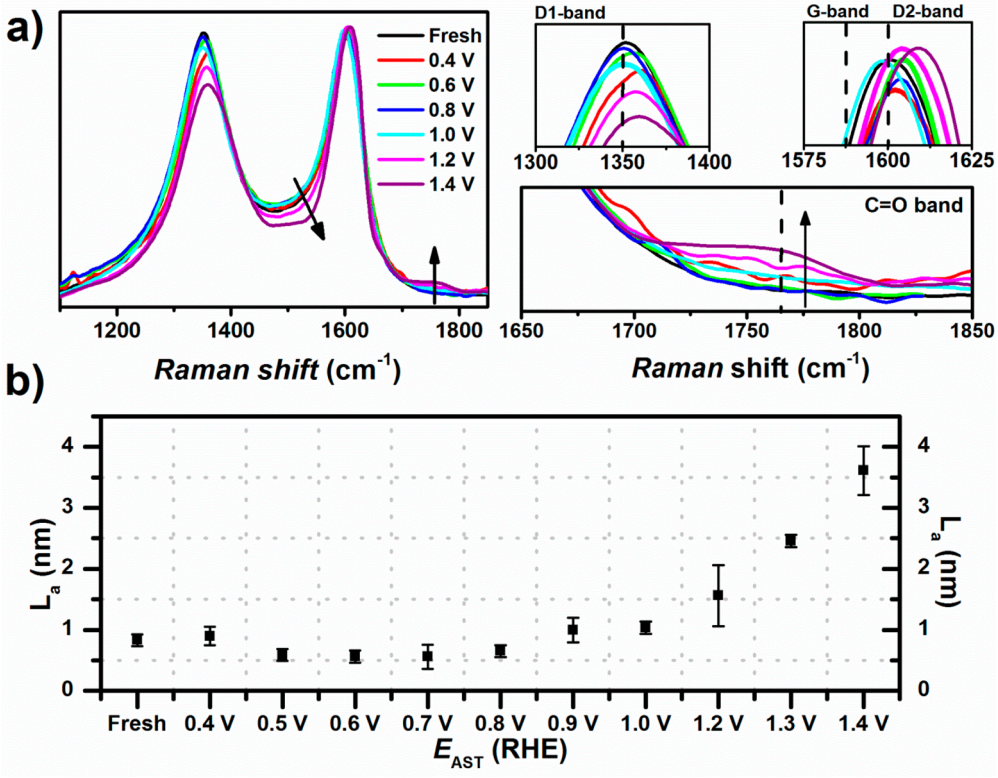

Figure 3. (a) Normalized Raman spectra of the fresh and aged Pt/HSAC electrocatalysts. Inset: D1-band, G-band, D2-band, and carbonyl band. (b) Variation of the carbon mean crystallite size (L_a) as a function of the polarization potential. Electrolyte: 0.1 M H_2SO_4; T = 330 K.

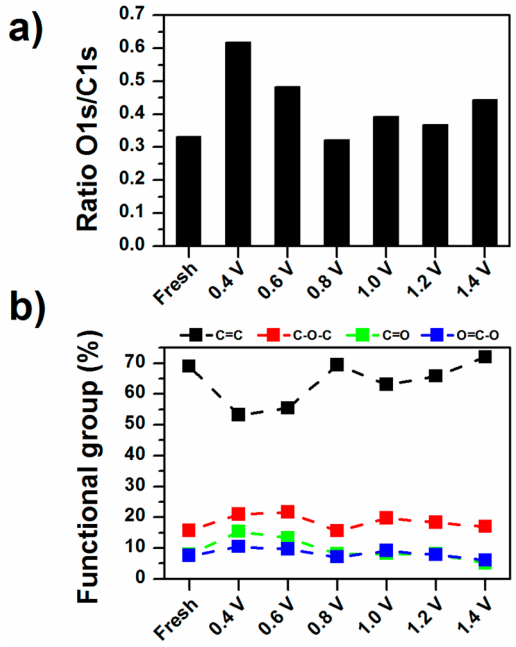

Figure 4. Variation of the (a) O1s/C1s atomic ratio and of the (b) concentration of the functional groups as a function of the polarization potential. Electrolyte: 0.1 M H_2SO_4; T = 330 K.

increased at E_{AST} = 0.40 V vs RHE but was depreciated for increasing polarization potentials up to 0.80 V vs RHE. As discussed previously, this can be rationalized by considering that the formation of oxygenated species on Pt nanoparticles (water splitting at E > 0.60 V vs RHE) catalyzes the oxidation of CO_{surf} groups into CO_2.[8,9,55]

Table 2. Values of the O1s/C1s Ratio Monitored by X-ray Photoelectron Spectroscopy, and Comparison to Literature Values

sample/ reference	description	ratio O1s/C1s
A	40 wt % Pt/HSAC TKK + water suspension	0.11
B	47 wt % Pt/HSAC TKK + water suspension + Nafion	0.52
C	40 wt % Pt/HSAC TKK + water suspension + Nafion + potential sweeping	0.33
D	fresh MEA cathode	0.17
6	Kangasniemi, K. H.; Condit, D. A.; Jarvi, T. D. *J. Electrochem. Soc.* **2004**, *151*, E125	0.07
56	Shao, Y.; Yin, G.; Gao, Y.; Shi, P. *J. Electrochem. Soc.* **2006**, *153*, A1093	0.03
54	Avasarala, B.; Moore, R.; Haldar, P. *Electrochim. Acta* **2010**, *55*, 4765	0.01
55	Álvarez, G.; Alcaide, F.; Miguel, O.; Cabot, P. L.; Martínez-Huerta, M. V.; Fierro, J. L. G. *Electrochim. Acta* **2011**, *56*, 9370	0.07

It is also striking to note that the concentration with CO_{surf} groups monitored by XPS and the structural changes monitored by Raman spectroscopy vary almost in parallel. Indeed, in the potential range 0.60 < E_{AST} < 0.80 V vs RHE, the observed decrease in D1-band intensity in Raman spectra (Figure 3) is nicely accompanied by a decreased oxygen content in XPS (Figure 4). This simply reflects that any structural defect is eager to chemisorb oxygen. Therefore, the preferential consumption of amorphous and defective graphite crystallites in this potential range translates into a decreased-CO_{surf} coverage. Similarly, at E_{AST} > 1.00 V vs RHE, the formation of structural defects on graphitic crystallites parallels the pronounced increase in oxygen content monitored in XPS.

dx.doi.org/10.1021/cs500449q | *ACS Catal.* 2014, 4, 2258−2267

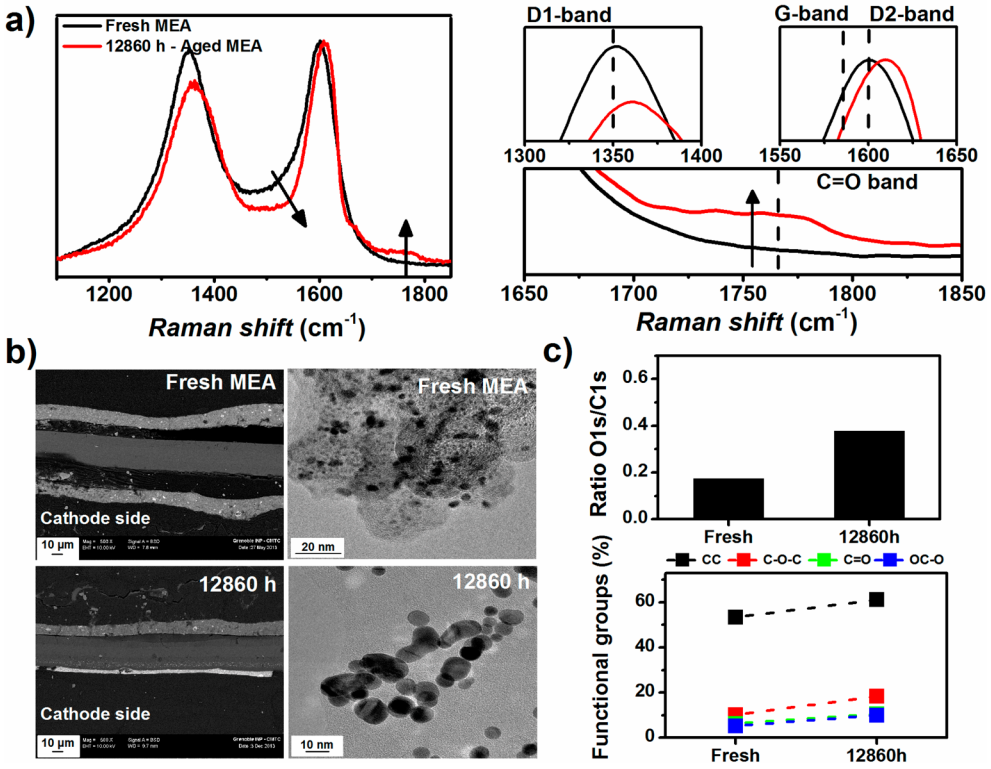

Figure 5. Characterization of MEAs operated under "real-life" PEMFC conditions: (a) Raman spectra, (b) scanning electron microscopy (SEM) and transmission electron microscopy (TEM) images, and (c) XPS-derived data. PEMFC operating conditions: j = 0.25 A cm^{-2}, 0.65 < E_{cell} < 0.77 V, 333 < T < 338 K, t = 12,860 h, 250 start/stop events.

Another important finding of this model study is the role of Nafion in promoting the COR. Table 2 displays the O1s/C1s ratio for electrodes prepared from different inks containing: (A) MQ-grade water + Pt/HSAC; (B) MQ-grade water + Pt/HSAC + Nafion, (C) MQ-grade water + Pt/HSAC + Nafion, this electrode being precycled in support electrolyte (10 potential cycles at v = 20 mV s^{-1} followed by one potential cycle at v = 100 mV s^{-1} and a CO_{ad} stripping voltammogram at v = 100 mV s^{-1}). The O1s/C1s ratio on the Pt/HSAC surface that contacted only MQ-grade water (0.11) is close to that monitored for reference samples in the literature (0.01−0.07).[6,56−58] However, this ratio increased to 0.52 in the presence of Nafion in the catalyst ink. In our former work,[48] we emphasized that, when Nafion superacidic and ion-conductive macromolecules contact the Pt/HSAC surface under air (during the ink and rotating-disk preparation), a mixed potential close to 0.95 V vs RHE is produced by the oxidation of the HSAC support (anode reaction) and the oxygen reduction at the Pt nanoparticles (cathode reaction). This in turn generates a time-dependent concentration of surface oxides on the HSAC surface (see XPS spectra taken after different ink storage durations on a Pt/Vulcan XC72 electrocatalyst in ref 48). On the contrary, in the absence of Nafion, the negligible ion conductivity of MQ-grade water prevents the formation of a galvanic cell in the catalyst ink, and limits the corrosion of the HSAC surface.

The effect of initial characterization CVs on the extent of oxidation of the HSAC surface is also worth noting. The O1s/C1s ratio observed on the electrochemically treated Pt/HSAC electrocatalyst decreases to 0.33 after electrochemical characterizations such as base or CO_{ads} stripping voltammograms (see Figure S4 in SI). This result suggests that any intermediate electrochemical characterization affects the surface state of Pt/HSAC electrocatalysts, in agreement with recent findings.[59] So as to lower their effect, only a small number of intermediary characterizations was performed (i.e., after 6, 24, 48, 72, and 96 h) during the AST.

Finally, the results obtained in model experiments (liquid electrolyte, T = 330 K, 96 h polarization) were compared to those derived from a PEMFC cathode aged in real operating conditions (solid polymer electrolyte, 333 < T < 338 K). For that purpose, a stack composed of 2 × 55 MEAs was operated on-site (i.e. with oxygen from the ambient air) at j = 0.25 A cm^{-2} and 333 < T < 338 K for t = 12,860 h. During the aging, the cell voltage was always between 0.65 < E_{cell} < 0.77 V (voltage decay rate ∼3.5 μV h^{-1}), and 250 start/stop events occurred during the operation of the PEMFC stack. The variation of the mean cell voltage (calculated on the 110 cells) at j = 0.25 A cm^{-2} is provided in Figure S5 in SI. Such a long-term PEMFC test places itself among the longest performed worldwide ever.[25,60−62] The changes in structure (monitored by Raman spectroscopy), in morphology (monitored by scanning and transmission electron microscopy), and in chemistry (monitored by X-ray photoelectron spectroscopy) of the Pt/HSAC cathode electrocatalyst are summarized in Figure 5. The Raman spectroscopy results (Figure 5a) confirm the preferential degradation of the disordered graphite domains of the HSAC supports, as shown by the decrease of the D1-band intensity and the thinning of the G- and D2-bands at 1610 cm^{-1}. The ordered graphite crystallites were also corroded (emergence of the carbonyl band at 1760 cm^{-1}). Figure 5b presents scanning electron microscopy (SEM) and transmission electron microscopy (TEM) images of the fresh/aged MEAs. The cathode thickness estimated from SEM images

dx.doi.org/10.1021/cs500449q | ACS Catal. 2014, 4, 2258−2267

decreased from 13.1 μm at the fresh state to 3.8 μm after 12,860 h of operation (−71% relative to the fresh cathode), in agreement with previous findings in the field.[1,13,22,23,28,29,32,63] Furthermore, the TEM images revealed an increased fraction of agglomerated Pt nanoparticles, as well as changes of the structure of the carbon particles. Those changes are in perfect agreement with what was observed on the model PEMFC electrocatalyst during the 96-h polarization (see TEM images, Pt particle size distribution, and the variation of the mean Pt particle size in Figure S6, Figure S7, and Table S1 of the SI). Finally, the concentration of CO_{surf} species and the O1s/C1s ratio monitored by X-ray photoelectron spectroscopy are presented in Figure 5c. The larger value of the O1s/C1s ratio indicates that, on average, the surface of the HSAC is more oxidized after 12,860 h of operation than at beginning of life. As stressed in the introduction, this trend has a great importance in terms of water management in the membrane electrode assembly. Indeed, a more oxidized HSAC support is less prone to evacuate water formed during the ORR, and may cause mass-transport losses[17,25,28,61] and even further accelerate the corrosion of the HSAC support/microporous layer.[22,30]

The combined physical, chemical, and electrochemical results presented in this study all point toward structure-sensitive COR kinetics on the HSAC supports used in PEMFCs. They provide first evidence that selective corrosion occurs on the disordered domains and the defective graphite crystallites in the potential range 0.40 < E_{AST} < 1.00 V vs RHE (Figure 6). Moreover, our results indicate that, during excursion in potential at E_{AST} > 1.00 V vs RHE, the ordered graphitic domains are also corroded.

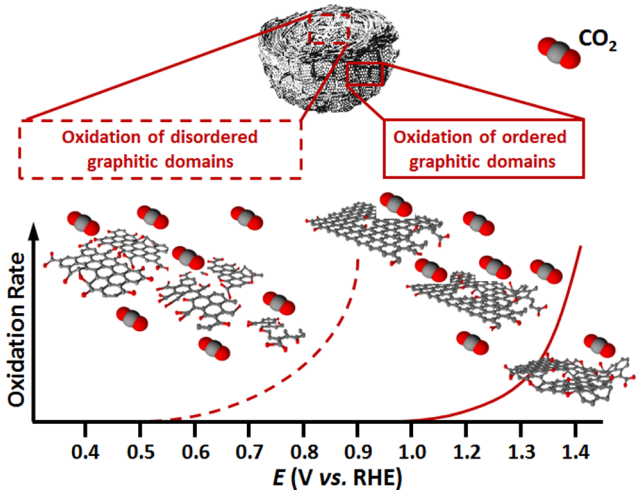

Figure 6. Schematic representation of the structure sensitivity of the COR kinetics on HSAC supports used in PEMFCs. The scheme representing the primary carbon particle is reproduced from reference 39 with permission of the International Union of Crystallography (http://dx.doi.org/10.1107/S0021889868004930).

For both disordered and ordered domains of the HSAC, the COR mechanism is believed to proceed via a similar mechanism, which involves the electrochemical formation of $C_{(s)}^{+}$ surface sites (eq 4). Those sites are then rapidly hydrolyzed into carbon surface oxides (eq 5), before being evolved into CO_2 (eq 6) as shown by the potential dependency of the surface oxide concentrations (Figure 4). This step is catalyzed by the presence of Pt nanoparticles (eq 7 and eq 8):[7,8,20,21]

$$C \rightarrow C^{+}_{(s)} + e^{-} \quad (4)$$

$$C^{+}_{(s)} + H_2O \rightarrow CO_{surf} + 2H^{+} + e^{-} \quad (5)$$

$$CO_{surf} + H_2O \rightarrow CO_2 + 2H^{+} + 2e^{-} \quad (6)$$

$$CO_{surf} + Pt \rightarrow Pt{-}CO_{ads} \quad (7)$$

$$Pt{-}CO_{ads} + H_2O \rightarrow CO_2 + 2H^{+} + 2e^{-} \quad (8)$$

In our former study, the structural changes occurring on a HSAC support during PEMFC operation at constant current (j = 0.6 A cm^{-2}) for 3,422 h suggested a structural dependence of the COR kinetics.[29] The results obtained in model and real PEMFC operating conditions strengthen and validate the proposed scenario on a 4-fold longer basis (12,860 h).

CONCLUSION

The degradation mechanisms of HSAC supports used in PEMFCs were investigated during long-term potentiostatic holds in a wide potential range from 0.40 to 1.40 V vs RHE. Our combined electrochemical and physicochemical findings suggest that the COR kinetics is structure-sensitive and proceeds more rapidly on the disordered domains of the HSAC support (amorphous carbon and defective graphite crystallites). Consequently:

(i) At low electrode potential (0.40 < E_{AST} < 1.00 V vs RHE), the amorphous carbon domains and the defective graphite crystallites present in the HSAC support are preferentially corroded. This phenomenon cannot be avoided during real PEMFC operation.

(ii) At high electrode potential (E_{AST} > 1.00 V vs RHE) encountered during open circuit potential, start/stop or fuel starvation events, the graphitic domains of the HSAC support are also prone to oxidation. Although these structural changes are mitigated during stationary PEMFC operation, the stack end-of-life can further be delayed in transient (e.g. start/stop) operation using appropriate materials and system modifications (see, e.g., ref 12 for more details).

These results suggest that the best possible mitigation strategies to prevent the COR on HSAC supports in real PEMFC operating conditions involves increasing their graphitic content,[15,51] modifying their chemistry,[24,64] or blocking the structural defects by halogen atoms or metal oxides so as to prevent their hydrolysis (eq 5).

ASSOCIATED CONTENT

Supporting Information

Further details of experimental methods, C1s and O1s X-ray photoelectron spectra, transmission electron micrograph and particle size distributions of the fresh and aged 40% wt. Pt/HSAC electrocatalysts, and mean cell voltage (calculated on the 110 cells) during the 12,860 h PEMFC aging test. This material is available free of charge via the Internet at http://pubs.acs.org.

AUTHOR INFORMATION

Corresponding Author

*E-mail: frederic.maillard@lepmi.grenoble-inp.fr

Notes

The authors declare no competing financial interest.

■ ACKNOWLEDGMENTS

This work was financially supported by Oseo-AII through the H2E project and by Bpi France. The authors gratefully acknowledge Alexandre Crisci of the CMTC (Consortium des Moyens Technologiques Communs) for the Raman spectroscopy measurements. M.C. thanks the Institut Universitaire de France for its support.

■ REFERENCES

(1) Dubau, L.; Castanheira, L.; Maillard, F.; Chatenet, M.; Lottin, O.; Maranzana, G.; Dillet, J.; Lamibrac, A.; Perrin, J.-C.; Moukheiber, E.; ElKaddouri, A.; De Moor, G.; Bas, C.; Flandin, L.; Caqué, N. *Wiley Interdiscip. Rev.: Energy Environ.* **2014**, DOI: 10.1002/wene.113.
(2) Kinoshita, K. *Carbon: Electrochemical and Physicochemical Properties*; John Wiley & Sons: New York, 1988.
(3) Kinoshita, K.; Bett, J. *Carbon* **1973**, *11*, 237−247.
(4) Kinoshita, K.; Bett, J. A. S. *Carbon* **1973**, *11*, 403−411.
(5) Kinoshita, K.; Bett, J. A. S. *Carbon* **1974**, *12*, 525−533.
(6) Kangasniemi, K. H.; Condit, D. A.; Jarvi, T. D. *J. Electrochem. Soc.* **2004**, *151*, E125−E132.
(7) Roen, L. M.; Paik, C. H.; Jarvi, T. D. *Electrochem. Solid-State Lett.* **2004**, *7*, A19−A22.
(8) Willsau, J.; Heitbaum, J. *J. Electroanal. Chem. Interfacial Electrochem.* **1984**, *161*, 93−101.
(9) Maillard, F.; Bonnefont, A.; Micoud, F. *Electrochem. Commun.* **2011**, *13*, 1109−1111.
(10) Reiser, C. A.; Bregoli, L.; Patterson, T. W.; Yi, J. S.; Yang, J. D. L.; Perry, M. L.; Jarvi, T. D. *Electrochem. Solid State Lett.* **2005**, *8*, A273−A276.
(11) Patterson, T. W.; Darling, R. M. *Electrochem. Solid State Lett.* **2006**, *9*, A183−A185.
(12) Dillet, J.; Spernjak, D.; Lamibrac, A.; Maranzana, G.; Mukundan, R.; Fairweather, J.; Didierjean, S.; Borup, R. L.; Lottin, O. *J. Power Sources* **2014**, *250*, 68−79.
(13) Durst, J.; Lamibrac, A.; Charlot, F.; Dillet, J.; Castanheira, L. F.; Maranzana, G.; Dubau, L.; Maillard, F.; Chatenet, M.; Lottin, O. *Appl. Catal., B* **2013**, *138*−*139*, 416−426.
(14) Meyers, J. P.; Darling, R. M. *J. Electrochem. Soc.* **2006**, *153*, A1432−A1442.
(15) Artyushkova, K.; Pylypenko, S.; Dowlapalli, M.; Atanassov, P. *J. Power Sources* **2012**, *214*, 303−313.
(16) Maillard, F.; Simonov, P.; Savinova, E. R. In *Carbon Materials for Catalysis*; Serp, P., Figueiredo, J. L., Eds.; John Wiley & Sons, Inc.: New York, 2009; Vol. 5, pp 429−480.
(17) Makharia, R.; Kocha, S. S.; Yu, P. T.; Sweikart, M. A.; Gu, W.; Wagner, F. T.; Gasteiger, H. *ECS Trans.* **2006**, *1*, 3−18.
(18) Cherstiouk, O. V.; Simonov, A. N.; Moseva, N. S.; Cherepanova, S. V.; Simonov, P. A.; Zaikovskii, V. I.; Savinova, E. R. *Electrochim. Acta* **2010**, *55*, 8453−8460.
(19) Ball, S. C.; Hudson, S. L.; Thompsett, D.; Theobald, B. *J. Power Sources* **2007**, *171*, 18−25.
(20) Stonehart, P. *Carbon* **1984**, *22*, 423−431.
(21) Maass, S.; Finsterwalder, F.; Frank, G.; Hartmann, R.; Merten, C. *J. Power Sources* **2008**, *176*, 444−451.
(22) Guilminot, E.; Corcella, A.; Charlot, F.; Maillard, F.; Chatenet, M. *J. Electrochem. Soc.* **2007**, *154*, B96−B105.
(23) Liu, Z. Y.; Brady, B. K.; Carter, R. N.; Litteer, B.; Budinski, M.; Hyun, J. K.; Muller, D. A. *J. Electrochem. Soc.* **2008**, *155*, B979−B984.
(24) Urchaga, P.; Weissmann, M.; Baranton, S.; Girardeau, T.; Coutanceau, C. *Langmuir* **2009**, *25*, 6543−6550.
(25) Cleghorn, S. J. C.; Mayfield, D. K.; Moore, D. A.; Moore, J. C.; Rusch, G.; Sherman, T. W.; Sisofo, N. T.; Beuscher, U. *J. Power Sources* **2006**, *158*, 446−454.
(26) Giordano, N.; Antonucci, P. L.; Passalacqua, E.; Pino, L.; Aricò, A. S.; Kinoshita, K. *Electrochim. Acta* **1991**, *36*, 1931−1935.
(27) United States Council for Automotive Research LLC, U.S.C.A.R. Fuel Cell Technical Team Technology Roadmap. http://www.uscar.org/guest/view_team.php?teams_id=17 (accessed 03/04/2014).
(28) Mathias, M. F.; Makharia, R.; Gasteiger, H.; Conley, J. J.; Fuller, T. J.; Gittleman, G. J.; Kocha, S. S.; Miller, D. P.; Mittelsteadt, C. K.; Xie, T.; Yan, S. G.; Yu, P. T. *Interface* **2005**, *14*, 24−35.
(29) Dubau, L.; Lopez-Haro, M.; Castanheira, L.; Durst, J.; Chatenet, M.; Bayle-Guillemaud, P.; Guétaz, L.; Caqué, N.; Rossinot, E.; Maillard, F. *Appl. Catal., B* **2013**, *142*−*143*, 801−808.
(30) Guilminot, E.; Corcella, A.; Chatenet, M.; Maillard, F.; Charlot, F.; Berthome, G.; Iojoiu, C.; Sanchez, J. Y.; Rossinot, E.; Claude, E. *J. Electrochem. Soc.* **2007**, *154*, B1106−B1114.
(31) Iojoiu, C.; Guilminot, E.; Maillard, F.; Chatenet, M.; Sanchez, J. Y.; Claude, E.; Rossinot, E. *J. Electrochem. Soc.* **2007**, *154*, B1115−B1120.
(32) Dubau, L.; Maillard, F.; Chatenet, M.; Guétaz, L.; André, J.; Rossinot, E. *J. Electrochem. Soc.* **2010**, *157*, B1887−B1895.
(33) Dubau, L.; Durst, J.; Maillard, F.; Chatenet, M.; Guétaz, L.; André, J.; Rossinot, E. *Fuel Cells* **2012**, *12*, 188−198.
(34) Sadezky, A.; Muckenhuber, H.; Grothe, H.; Niessner, R.; Pöschl, U. *Carbon* **2005**, *43*, 1731−1742.
(35) Knight, D. S.; White, W. B. *J. Mater. Res.* **1989**, *4*, 385−393.
(36) Yoda, T.; Uchida, H.; Watanabe, M. *Electrochim. Acta* **2007**, *52*, 5997−6005.
(37) Park, Y.-C.; Kakinuma, K.; Uchida, M.; Tryk, D. A.; Kamino, T.; Uchida, H.; Watanabe, M. *Electrochim. Acta* **2013**, *91*, 195−207.
(38) Park, Y.-C.; Kakinuma, K.; Uchida, M.; Uchida, H.; Watanabe, M. *Electrochim. Acta* **2014**, *123*, 84−92.
(39) Heidenreich, R. D.; Hess, W. M.; Ban, L. L. *J. Appl. Crystallogr.* **1968**, *1*, 1−19.
(40) Mathis, W. *J. Power Sources* **2006**, *156*, 142−150.
(41) Jawhari, T.; Roid, A.; Casado, J. *Carbon* **1995**, *33*, 1561−1565.
(42) Nemanich, R. J.; Solin, S. A. *Phys. Rev. B* **1979**, *20*, 392−401.
(43) Lespade, P.; Al-Jishi, R.; Dresselhaus, M. S. *Carbon* **1982**, *20*, 427−431.
(44) Tuinstra, F.; Koenig, J. L. *J. Chem. Phys.* **1970**, *53*, 1126−1130.
(45) Nakamizo, M.; Honda, H.; Inagaki, M. *Carbon* **1978**, *16*, 281−283.
(46) Nakamizo, M.; Tamai, K. *Carbon* **1984**, *22*, 197−198.
(47) Gruber, T.; Zerda, T. W.; Gerspacher, M. *Carbon* **1994**, *32*, 1377−1382.
(48) Zhao, Z.; Castanheira, L.; Dubau, L.; Berthomé, G.; Crisci, A.; Maillard, F. *J. Power Sources* **2013**, *230*, 236−243.
(49) Sze, S. K.; Siddique, N.; Sloan, J. J.; Escribano, R. *Atmos. Environ.* **2001**, *35*, 561−568.
(50) Hiramitsu, Y.; Sato, H.; Hosomi, H.; Aoki, Y.; Harada, T.; Sakiyama, Y.; Nakagawa, Y.; Kobayashi, K.; Hori, M. *J. Power Sources* **2010**, *195*, 435−444.
(51) Hara, M.; Lee, M.; Liu, C.-H.; Chen, B.-H.; Yamashita, Y.; Uchida, M.; Uchida, H.; Watanabe, M. *Electrochim. Acta* **2012**, *70*, 171−181.
(52) Bruna, M.; Borini, S. *Phys. Rev. B: Condens. Mater. Phys.* **2010**, 81.
(53) Pimenta, M. A.; Dresselhaus, G.; Dresselhaus, M. S.; Cançado, L. G.; Jorio, A.; Saito, R. *Phys. Chem. Chem. Phys.* **2007**, *9*, 1276−1291.
(54) Cançado, L. G.; Takai, K.; Enoki, T.; Endo, M.; Kim, Y. A.; Mizusaki, H.; Jorio, A.; Coelho, L. N.; Magalhães-Paniago, R.; Pimenta, M. A. *Appl. Phys. Lett.* **2006**, *88*, 163106.
(55) Li, W.; Lane, A. M. *Electrochem. Commun.* **2009**, *11*, 1187−1190.
(56) Avasarala, B.; Moore, R.; Haldar, P. *Electrochim. Acta* **2010**, *55*, 4765−4771.
(57) Álvarez, G.; Alcaide, F.; Miguel, O.; Cabot, P. L.; Martínez-Huerta, M. V.; Fierro, J. L. G. *Electrochim. Acta* **2011**, *56*, 9370−9377.
(58) Shao, Y.; Yin, G.; Gao, Y.; Shi, P. *J. Electrochem. Soc.* **2006**, *153*, A1093−A1097.
(59) Castanheira, L.; Dubau, L.; Maillard, F. *Electrocatalysis* **2014**, *5*, 125−135.
(60) St-Pierre, J.; Jia, N. Y. *J. New Mater. Electrochem. Syst.* **2002**, *5*, 263−271.
(61) Liu, D.; Case, S. *J. Power Sources* **2006**, *162*, 521−531.

(62) de Bruijn, F. A.; Dam, V. A. T.; Janssen, G. J. M. *Fuel Cells* **2008**, *8*, 3−22.
(63) Gallagher, K.; Darling, R.; Fuller, T. In *Handbook of Fuel Cells - Fundamentals, Technology and Applications*; Vielstich, W., Yokokawa, H., Gasteiger, H. A., Eds.; John Wiley & Sons, Ltd.: New York, 2009; Vol. *6*, pp 819−828.
(64) Shao, Y.; Sui, J.; Yin, G.; Gao, Y. *Appl. Catal., B* **2008**, *79*, 89−99.